Solution Structure of the E-Domain of Staphylococcal Protein A‡

Melissa A. Starovasnik,§ Nicholas J. Skelton,§ Mark P. O'Connell,§ Robert F. Kelley,§ Dorothea Reilly,|| and Wayne J. Fairbrother*,§

Departments of Protein Engineering and Cell Culture, Genentech, Inc., 460 Point San Bruno Boulevard, South San Francisco, California 94080

Received June 13, 1996; Revised Manuscript Received October 3, 1996⊗

ABSTRACT: The E-domain of staphylococcal protein A is one of five homologous IgG-binding domains designated E, D, A, B, and C that comprise the extracellular portion of protein A. The E-domain binds tightly to Fc fragments of IgG and binds certain Fv fragments with micromolar affinity. To explore further the structural features of Fc binding by protein A, and as a first step in developing a structural understanding of E-domain/Fv complex formation, we have determined the solution structure of the uncomplexed E-domain using 2D homonuclear and heteronuclear NMR spectroscopy. Complete ^{1}H and ^{15}N resonance assignments were obtained, and the structure was determined from 383 NOE-derived distance restraints, 34 ϕ and 19 χ_1 dihedral angle restraints, and 54 restraints for 27 H-bonds. $^3J_{H^\alpha-H^\beta}$ coupling constants and long-range NOEs involving Phe11 indicate the side chain exists in more than one conformation with differing χ_1 values. NOE restraints that were incompatible with $\chi_1 = -60°$ were removed from one set of structure calculations, and those incompatible with $\chi_1 = 180°$ were removed from a second set to allow Phe11 to explore both rotamer wells. Thus, two sets of 20 final structures, having no distance or dihedral angle restraint violations greater than 0.12 Å or 1.6°, respectively, represent the solution structure of the E-domain. Backbone atomic rms differences with respect to the mean coordinates for each set of 20 structures for residues 8−53 averaged 0.41 ± 0.06 and 0.35 ± 0.06 Å. No significant differences in the overall structure result from the different orientations of Phe11. The solution structure of the E-domain consists of three α-helices that pack together to form a compact helical bundle. A detailed comparison between the E-domain ensembles and the previously determined structure for the B-domain in complex with Fc indicates that only the 180° χ_1 rotamer of Phe11 is competent for binding; the −60° χ_1 rotamer must reorient to 180° to create a cavity that is filled by Ile253 from the CH_2 domain of Fc in the Fc-bound complex.

Staphylococcal protein A is a pathogenicity factor found on the surface of *Staphylococcus aureus* [for review see Langone (1982)]. Protein A has long been utilized as a powerful immunological tool on the basis of its ability to bind tightly to the Fc region of IgG. The role of protein A in *S. aureus* is not well understood, but it is thought to enhance infectivity by coating the cell with host IgG molecules in an effort to evade the host immune system. The gene for protein A encodes a total of 524 residues, including an N-terminal signal sequence, five homologous ∼58 residue IgG-binding domains, and a C-terminal region containing the site for cell wall attachment (Uhlén et al., 1984; Moks et al., 1986). The IgG-binding domains are designated E, D, A, B, and C, in order from the N-terminus, and are 65−90% identical to one another (Figure 1).

The structure of the B-domain has been determined previously both in complex with an Fc antibody fragment by X-ray crystallography (Deisenhofer et al., 1978; Deisenhofer, 1981) and free in solution by NMR[1] spectroscopy [Torigoe et al., 1990; Gouda et al., 1992; reviewed in Tashiro and Montelione (1995)]. The X-ray structure, refined to 2.8 Å resolution, includes two α-helices, helix 1 (residues 7−15, E-domain numbering)[2] and helix 2 (residues 23−34), oriented antiparallel to one another ($\Omega = 179°$). Weak electron density was present for residues 39−45, and residues 46−56 were not included in the model. Residues from both helix 1 and helix 2 of the B-domain were found to contact Fc in the complex. The structure of the uncomplexed B-domain in solution contains three α-helices; the first two are in general agreement with the crystal structure of the Fc-bound B-domain (helix 1, residues 7−16; helix 2, residues 22−34) although their relative orientation is significantly different ($\Omega = -150°$), and the third helix comprises residues 39−52.

Thus, two major differences are apparent between the two B-domain structures: the presence or absence of helix 3 and the relative orientations of helices 1 and 2. Whether the observed differences are a direct consequence of Fc binding

‡ Coordinates for the final ensemble and minimized mean structures have been deposited in the Brookhaven Protein Data Bank under the file names 1EDI, 1EDJ, 1EDK, and 1EDL.

* To whom correspondence should be addressed.
§ Department of Protein Engineering.
|| Department of Cell Culture.

⊗ Abstract published in *Advance ACS Abstracts,* November 15, 1996.

[1] Abbreviations: 2Q, double quantum; COSY, correlation spectroscopy; COSY-35, COSY with 35° mixing pulse, rather than 90°; DG, distance geometry; DSS, 3-(trimethylsilyl)-1-propane-*1,1,2,2,3,3-d*$_6$-sulfonic acid; EDTA, ethylenediaminetetraacetic acid; HSQC, heteronuclear single-quantum coherence; k_{off}, dissociation rate constant; k_{on}, association rate constant; NOE, nuclear Overhauser effect; NOESY, 2D NOE spectroscopy; NMR, nuclear magnetic resonance; PBS, phosphate-buffered saline; rMD, restrained molecular dynamics; rms, root mean square; S^{ang}, angular order parameter; SD, standard deviation; TOCSY, total correlation spectroscopy; TPPI, time-proportional phase incrementation; Z-domain, B-domain G27A point mutant.

[2] E-Domain numbering is used throughout the text when discussing B-domain residues.

S0006-2960(96)01409-2 CCC: $12.00

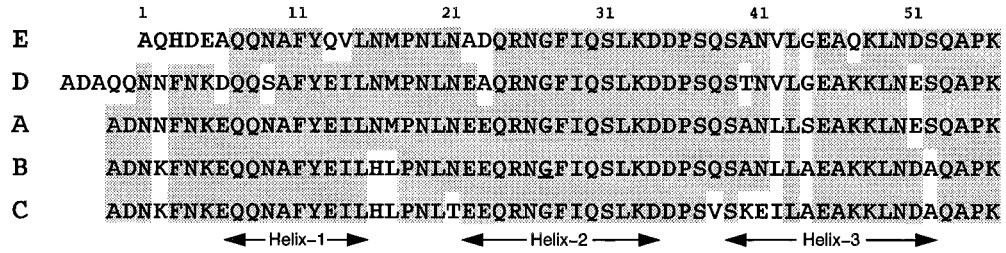

FIGURE 1: Sequence alignment of protein A IgG-binding domains. Conserved residues are shaded. The N-terminal 291 residues of native staphylococcal protein A are shown (Moks et al., 1986). The G27A substitution in the B-domain that represents the Z-domain is underlined. The N-terminal residue of B- and Z-domains used for the binding measurements reported here is valine rather than the native alanine.

or result from the different methods and conditions used to determine the structures is unclear. Recent amide/solvent exchange measurements of the Fc-bound B-domain and circular dichroism measurements of an Fc-bound B-domain variant (that contains only one mutation within the three-helix bundle, G27A, designated Z-domain; Nilsson et al., 1987) indicate that the third helix is present in solution when bound to Fc, suggesting that the absence of this helix from the crystal structure is artifactual (Gouda et al., 1992; Jendeberg et al., 1996). The different helix 1/helix 2 orientations have been interpreted as evidence for a conformational change upon binding of the B-domain to Fc (Gouda et al., 1992). A conformational change upon binding is also supported by kinetic data that show reduced on-rates relative to the diffusion limit (Jendeberg et al., 1995). However, a recent preliminary NMR structure of the Z-domain shows only a small difference in the orientation of helix 1 and helix 2 relative to the Fc-bound state of the B-domain [$\Omega \approx -170°$ for the Z-domain, as reported by Jendeberg et al. (1996), compared to $\Omega = 179°$ for the Fc-bound B-domain]. Given their nearly identical primary sequences and similar binding properties (Nilsson et al., 1987), B- and Z-domains are expected to adopt very similar tertiary structures. The different helix 1/helix 2 angles described for the free states of these two proteins therefore are surprising and raise questions regarding the significance of the previously reported change in the helix 1/helix 2 angle upon Fc binding.

To explore further the conformational properties of protein A domains, we have determined the structure of the most N-terminal domain of protein A, the E-domain. The E-domain (56 residues) shares 71% amino acid identity with the B-domain (Figure 1) and not only binds Fc fragments but also binds with micromolar affinity to Fv fragments containing a type III V_H domain (M. P. O'Connell and R. F. Kelley, unpublished results). Complete ^{1}H and ^{15}N resonance assignments were obtained, and three-dimensional structures were calculated. The solution structure of the E-domain of protein A is presented and compared with the previously determined structures of the B-domain.

MATERIALS AND METHODS

Materials. Celtone-N and Celtone-C were purchased from Martek, Inc. Enriched [$^{13}C_6$]-D-glucose (>99%) and enriched [^{15}N]ammonium chloride (>99%) were purchased from Isotec, Inc.

Protein Expression. The E-domain was expressed in *Escherichia coli* from plasmid pProAEDom, which employs an alkaline phosphatase promoter and an STII signal sequence for secretion into the periplasm (Chang et al., 1987). Unlabeled protein was obtained from cell paste derived from a 10 L fermentation. Production of ^{15}N-labeled protein in shake flasks was essentially as described (Reilly & Fairbrother, 1994), except that a *prl* mutant of strain W3110 was used and cells were grown at 30 °C to obtain optimal protein expression. The fractionally ^{13}C-labeled E-domain was produced from cells grown in the presence of 15% uniformly labeled [$^{13}C_6$]-D-glucose and 85% D-glucose at natural isotope abundance.

The E-domain was purified from both the culture medium and the periplasmic shockate. The medium was loaded directly onto an IgG−Sepharose column (Pharmacia) pre-equilibrated in 10 mM Tris, pH 7.5, and 150 mM NaCl and eluted from the resin using 0.1 M acetic acid, pH 3. The cell pellet was osmotically shocked by resuspension in 10 mM Tris, pH 7.5, and 1 mM EDTA to release the soluble periplasmic contents. The suspension was stirred at 4 °C for 30 min and then centrifuged, and the supernatant was loaded onto the IgG−Sepharose column. Typical combined yields from the culture medium and periplasmic shockate were 20 mg/L of cell culture. Protein was >95% pure as determined by SDS−polyacrylamide gel electrophoresis. Purified protein samples were verified, and isotope incorporation levels were determined by electrospray mass spectrometry.

NMR samples were prepared by dialyzing the E-domain into NMR sample buffer (10 mM phosphate, 150 mM NaCl, pH 5.7, 0.1 mM EDTA, 0.1 mM NaN_3) and concentrating either by lyophilization or using Centricon-SR3 (Millipore) concentration cells.

The B-domain (see Figure 1) and "Z-domain" (a single point mutant of the B-domain, G27A) were expressed and purified essentially as described above for the E-domain.

Binding Kinetics. Association and dissociation rate constants for Fc binding by E-, B-, and Z-domains were determined by surface plasmon resonance using a BIAcore 1000 (Pharmacia Biosensor). CD4−Fc_1 fusion protein (Capon et al., 1989) was immobilized on a biosensor chip covalently through the primary amines (Johnsson et al., 1991). CD4−Fc_1 was used rather than full-length IgG to avoid complications from weak binding to the Fab portion (Langone, 1982). A low coupling density of 2600 RUs was used for both association and dissociation constant determinations. Association and dissociation rates were measured at flow rates of 25 μL/min, in PBS buffer (pH 7.4) with 0.05% Tween 20 (Karlsson et al., 1991). Dissociation rates were measured with saturating injections at a concentration of 25 μM. Reported values for k_{off} are the mean ± SD of five measurements. Association rate constants were derived from measurements at four different concentrations, 1 μM, 750 nM, 500 nM, and 250 nM, that

were fit independently. The reported values are mean ± SD for the four concentrations.

NMR Spectroscopy. All spectra were acquired on a Bruker AMX-500 spectrometer at 25 °C unless indicated otherwise. Standard pulse sequences and phase cycling were employed to record the following spectra in 92% H_2O/8% D_2O solution: COSY (Aue et al., 1975), TOCSY (Braunschweiler & Ernst, 1983; Bax & Davis, 1985) with a spin-lock period of 70 ms, NOESY (Kumar et al., 1980; Bodenhausen et al., 1984) with mixing times of 50, 100, and 150 ms, and NOESY at 20 °C with a mixing time of 150 ms. The "clean" DIPSI-2rc sequence was used for isotropic mixing in the TOCSY spectrum (Cavanagh & Rance, 1992). In addition, the following spectra were recorded in 99.99% D_2O solution: COSY-35, 2Q (Braunschweiler et al., 1983; Rance & Wright, 1986), and NOESY with a mixing time of 100 ms. All 2D spectra were recorded in a phase-sensitive manner using time-proportional phase incrementation for quadrature detection in t_1 (Marion & Wüthrich, 1983). Presaturation of the water resonance was used for solvent suppression. All TOCSY and NOESY spectra were acquired with the addition of a short Hahn-echo period to improve the quality of both the solvent suppression and the baseline (Rance & Byrd, 1983; Davis, 1989). Chemical shifts were referenced to internal DSS.

The following heteronuclear experiments were acquired using the uniformly ^{15}N-labeled E-domain in 92% H_2O/8% D_2O: HSQC and 2D HSQC-TOCSY with enhanced sensitivity using a PEP-Z-HSQC sequence (Cavanagh et al., 1991; Akke et al., 1994) and a TOCSY mixing time of 89 ms. Quadrature detection in t_1 was obtained using the TPPI−States method (Marion et al., 1989). Spin-lock purge pulses were employed for water suppression in all heteronuclear experiments (Messerle et al., 1989). In addition, a $^1H/^{13}C$ HSQC spectrum was acquired on a sample containing 14% ^{13}C incorporation dissolved in 99.99% D_2O at 20 °C to enable unambiguous stereospecific assignments for the methyl groups of leucine and valine (Neri et al., 1989; Senn et al., 1989).

HSQC spectra for measuring amide hydrogen/deuterium exchange kinetics were acquired at 13 °C using the PEP-Z-HSQC pulse sequence (Akke et al., 1994). Acquisition of the first HSQC experiment was initiated ∼8 min after lyophilized protein was dissolved in D_2O. Initial spectra were acquired using four transients per increment with a total acquisition time of 12 min.

Distance and Dihedral Restraints. Assigned NOE cross-peaks from the 100 ms NOESY spectra acquired in H_2O and D_2O were characterized as strong, medium, or weak, corresponding to upper bound distance restraints of 3.0, 4.0, and 5.0 Å, respectively. The upper bound distance restraints assigned to overlapped cross-peaks were either increased by 1 Å or set to the maximum upper bound (5 Å), depending on a qualitative assessment of the severity of overlap. Lower bounds between nonbonded atoms were set to the sum of their van der Waals radii. Pseudoatom corrections were added to interproton distance restraints where necessary (Wüthrich et al., 1983). A 0.5 Å correction was added to the upper bound for restraints involving methyl protons (Tropp, 1980; Koning et al., 1990). $\langle r^{-6} \rangle$ averaging was applied to restraints involving degenerate protons from aromatic rings and methylene groups (Brünger et al., 1986; Clore et al., 1986) and to allow the use of NOEs that were ambiguous due to resonance overlap in the 2D NOESY spectra.

$^3J_{H^N-H^\alpha}$ coupling constants were determined using a Levenberg−Marquardt line-fitting algorithm (Press et al., 1986) to measure splittings from the antiphase double-Lorentzian cross sections of H^N-H^α cross-peaks in a COSY spectrum processed with high digital resolution in F_2. ϕ angle restraints of $-90° < \phi < -40°$ and $-150° < \phi < -90°$ were imposed for residues with $^3J_{H^N-H^\alpha}$ <6.0 Hz and >8.5 Hz, respectively. χ_1 restraints and stereospecific assignments for β-methylene groups were based on $^3J_{H^\alpha-H^\beta}$ coupling constants measured from a COSY-35 spectrum and examination of intraresidue NOEs in a 50 ms NOESY spectrum (Wagner et al., 1987). In some cases, stereospecific assignments and χ_1 restraints were not added until after preliminary structures were calculated and the χ_1 rotamer was well-defined without explicitly including them as input restraints.

Hydrogen bond restraints were based upon observation of slow amide proton/deuterium exchange. Hydrogen bond restraints for backbone atoms were included only if a hydrogen bond was observed in greater than 50% of the converged structures resulting from initial structure calculations performed in the absence of such restraints. Each hydrogen bond identified was defined using two distance restraints: $r_{NH-O} = 1.7-2.4$ Å and $r_{N-O} = 2.5-3.4$ Å.

Structure Calculations. Distance geometry (DG) calculations were carried out using the program DGII (Havel, 1991) within INSIGHT II (Biosym Technologies, Inc., San Diego). Following triangle and tetrangle bounds smoothing, distance matrices were generated using random metrization, and coordinates satisfying the trial distances were obtained by prospective embedding and majorization in four dimensions. The embedded structures were then optimized by simulated annealing in four dimensions and conjugate gradient minimization in three dimensions (Havel, 1991) using the CVFF parameters.

Converged DG structures were refined with restrained molecular dynamics (rMD) using DISCOVER (Biosym Technologies, Inc., San Diego). The all-atom AMBER force field (Weiner et al., 1984, 1986) was used with a 10.0 Å cutoff for nonbonded interactions and a distance-dependent dielectric constant ($\epsilon = 4r$) to compensate for the lack of explicit solvent. Side-chain charges on Asp, Glu, Arg, and Lys residues were scaled by multiplying the default charges by 0.2 in order to reduce artifacts due to excessive charge−charge interactions. The NOE distance restraints, hydrogen bond distance restraints, and dihedral angle restraints were applied using a square-well potential function (Kessler et al., 1988) with force constants of 25 kcal·mol^{-1}·Å^{-2}, 25 kcal·mol^{-1}·Å^{-2}, and 100 kcal·mol^{-1}·rad^{-2}, respectively. Additional ω restraints ($-170° < \omega < 170°$, force constant 64 kcal·mol^{-1}·rad^{-2}) were included as a supplement to the force field to maintain peptide planarity and were not included in the dihedral angle restraint violation analysis given in Table 2. Each of the converged DG structures was initially minimized using 100 steps of steepest descents minimization, followed by 1000 steps of conjugate gradient minimization. The structures were then equilibrated at 1000 K for 1 ps, with the distance and dihedral angle restraint force constants (as indicated above) scaled by a factor of 0.1. The experimental restraint force constants were in

Table 1: Fc Binding Kinetics of Protein A Domains[a]

protein	k_{on}, $\times 10^5$ M^{-1} s^{-1}	k_{off}, s^{-1}	K_d, nM
E-domain	4.3 ± 0.6	0.048 ± 0.002	110 ± 20
B-domain	5.6 ± 1.2	0.020 ± 0.001	36 ± 9
Z-domain	5.4 ± 0.3	0.017 ± 0.001	31 ± 4

[a] Binding kinetics were measured to the CD4−Fc_1 fusion protein by surface plasmon resonance as described in Materials and Methods. Rate constants are given as the mean ± SD for independent measurements. K_d is calculated from k_{off}/k_{on}.

creased to their full values during the next 2 ps. The system remained at 1000 K for a further 1 ps before being cooled to 0 K over 6 ps. Following another 1 ps at 0 K the system was again minimized for 100 cycles of steepest descents and 2000 steps of conjugate gradient minimization. Out-of-plane energies were scaled by a factor of 2.0 throughout. All calculations were performed on a Silicon Graphics Challenge XL computer.

RESULTS

Fc-Binding Kinetics of the E-Domain. The kinetics of E-domain binding to Fc were assessed by surface plasmon resonance. CD4−Fc_1 fusion protein (Capon et al., 1989) was coupled to the biosensor chip. Protein A was previously shown to not interact with CD4 (Jendeberg et al., 1995). Rate constants are given in Table 1. The rate constants are similar to those previously reported for the Z-domain (Jendeberg et al., 1995, Braisted & Wells, 1996), with small differences potentially resulting from the reduced coupling density used here. The B-domain has indistinguishable binding constants from those of the Z-domain, as expected. The on-rate for the E-domain is essentially the same as that for the B- and Z-domains, although the off-rate is approximately 3-fold faster.

NMR Measurements. The uncomplexed E-domain is relatively unstable and at millimolar concentrations aggregates slowly over a period of days. Therefore, our analysis was limited to 2D NMR methods where data acquisition times were kept to a minimum. Depending on protein concentration and temperature, an initially very soluble (1−3 mM) NMR sample would be transformed into a highly viscous gel. In several cases, it was necessary to regenerate the NMR sample by dissolving the gel in 6 M GuHCl and dialyzing the protein into NMR sample buffer. This procedure yielded about 80% recovery.

E-Domain ^1H resonances were assigned by conventional homonuclear 2D NMR methods (Wüthrich, 1986; Chazin & Wright, 1988). Spin systems were initially assigned through analysis of COSY and TOCSY spectra and later confirmed with a $^1H/^{15}N$ HSQC-TOCSY spectrum. Degenerate chemical shifts within amino acid spin systems were identified using the 2Q spectrum (Chazin et al., 1988). Sequence-specific resonance assignments were obtained from analysis of sequential NOE connectivities observed in NOESY spectra acquired at 25 and 20 °C to resolve ambiguities due to resonance overlap. The fingerprint region of the COSY spectrum and the amide region of the NOESY spectrum used for obtaining assignments are shown in Figure 2. ^{13}C resonances for the methyl groups of valines and leucines were assigned on the basis of their ^1H chemical shifts by inspection of a $^1H/^{13}C$ HSQC spectrum obtained from a sample with 14% ^{13}C enrichment. Complete ^{15}N resonance

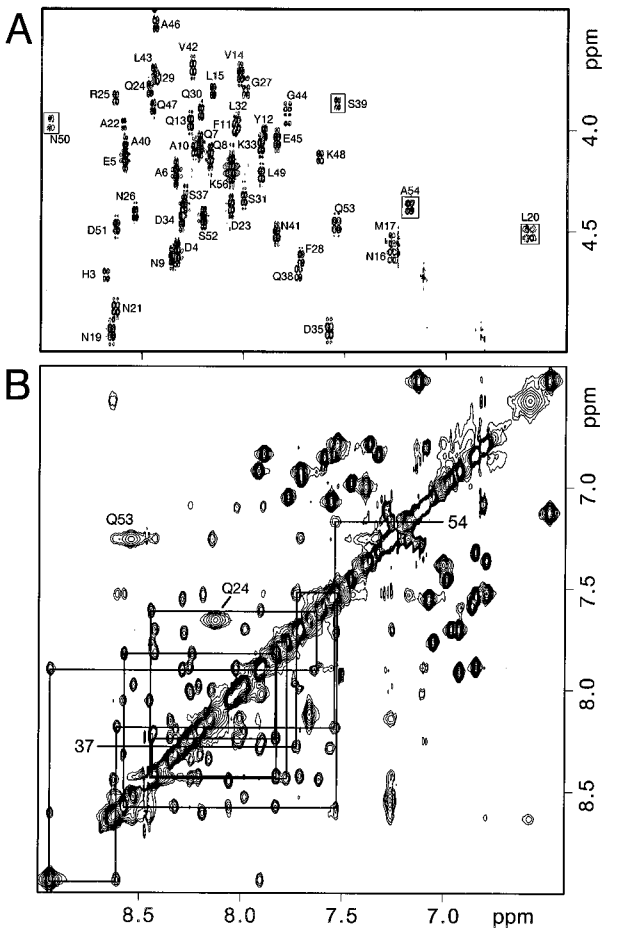

FIGURE 2: NMR spectra of the E-domain acquired at 25 °C, pH 5.7. (A) H^N-H^α fingerprint region of the COSY spectrum. Assignments are indicated. The four boxed peaks are plotted at a lower level than the rest of the spectrum. (B) Amide proton region of a 100 ms NOESY spectrum. Consecutive d_{NN} connectivities observed for residues 37−54 are indicated. $H^{\epsilon 21}/H^{\epsilon 22}$ cross-peaks for Gln24 and Gln53 are labeled to highlight their unusual chemical shifts.

assignments were obtained through analysis of a 2D $^1H/^{15}N$ HSQC-TOCSY spectrum and comparison with previously assigned ^1H frequencies. Resonance assignments are listed in Supporting Information (Table S1).

Forty-one $^3J_{H^N-H^\alpha}$ coupling constants were measured from a COSY spectrum acquired at 25 °C; 29 residues had $^3J_{H^N-H^\alpha} < 6$ Hz and 5 had $^3J_{H^N-H^\alpha} > 8.5$ Hz (Figure 3). $^3J_{H^\alpha-H^\beta}$ coupling constants were determined from a COSY-35 spectrum for 29 of 41 β-methylene containing spin systems. χ_1 restraints for 19 residues were derived, and stereospecific assignments for the β protons of 10 of those residues were determined. Stereospecific assignments were obtained for the methyl groups of both valine residues and four of the five leucine residues based on the ^{13}C splittings observed in a $^1H/^{13}C$ HSQC acquired on a 14% ^{13}C-labeled sample (Neri et al., 1989; Senn et al., 1989); the remaining leucine (Leu43) has degenerate methyl ^1H chemical shifts. Protons protected from exchange with solvent at 13 °C, pH 5.7, were identified for 37 backbone amides (Figure 3) and seven pairs of side-chain amides arising from Gln13, Asn16, Asn19, Asn21, Gln24, Asn50, and Gln53.

Structure Determination. Initial structures were calculated using only NOE-derived distance restraints and dihedral angle restraints. Examination of these preliminary structures

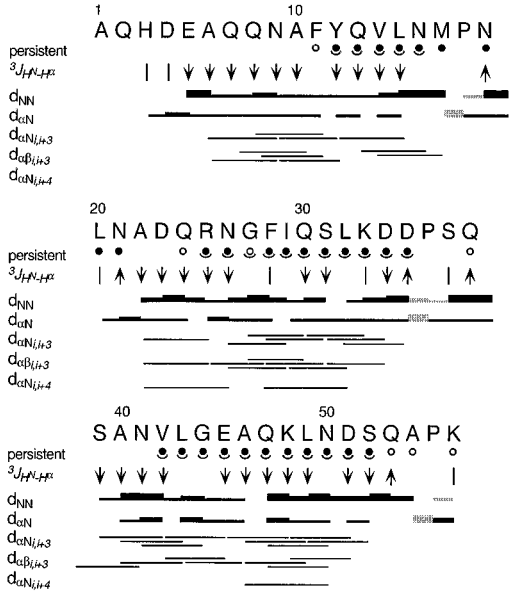

FIGURE 3: Summary of sequential connectivities, amide proton exchange, and coupling constants. The relative intensities of the sequential NOEs are indicated by the thickness of the bars between adjacent residues. Sequential connectivities involving the H^δ of proline residues are denoted by shaded bars. The sequential connectivity diagram is incomplete due to overlap in the 2D NOESY spectrum. Persistent refers to whether the amide proton was detected in an HSQC spectrum acquired after the sample had been lyophilized from H_2O and redissolved in D_2O. Open circles indicate the proton was detected 14 min after solubilization; filled circles indicate the proton could still be detected 2 h after solubilization. Underlined circles indicate that an α-helical hydrogen bond restraint was added for this proton. ↓ indicates $^3J_{H^N-H^\alpha} < 6.0$ Hz; ↑ indicates $^3J_{H^N-H^\alpha} > 8.5$ Hz; | indicates 6.0 Hz $< {}^3J_{H^N-H^\alpha} <$ 8.5 Hz.

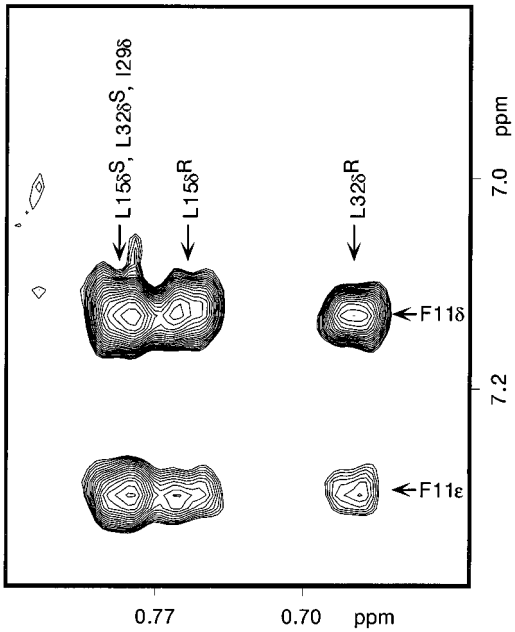

FIGURE 4: Methyl to aromatic proton region of the 2D D_2O NOESY spectrum of the E-domain, mixing time 100 ms. NOE cross-peaks between Phe11 and the *pro-R* methyl groups of Leu15 and Leu32 are indicated. Cross-peaks between Phe11 and the *pro-S* methyl groups of Leu15 and Leu32 and the δ-methyl group of Ile29 are ambiguous and were not used to generate restraints for the structure calculations.

indicated the presence of three α-helices, consistent with the observed patterns of sequential and medium-range NOE

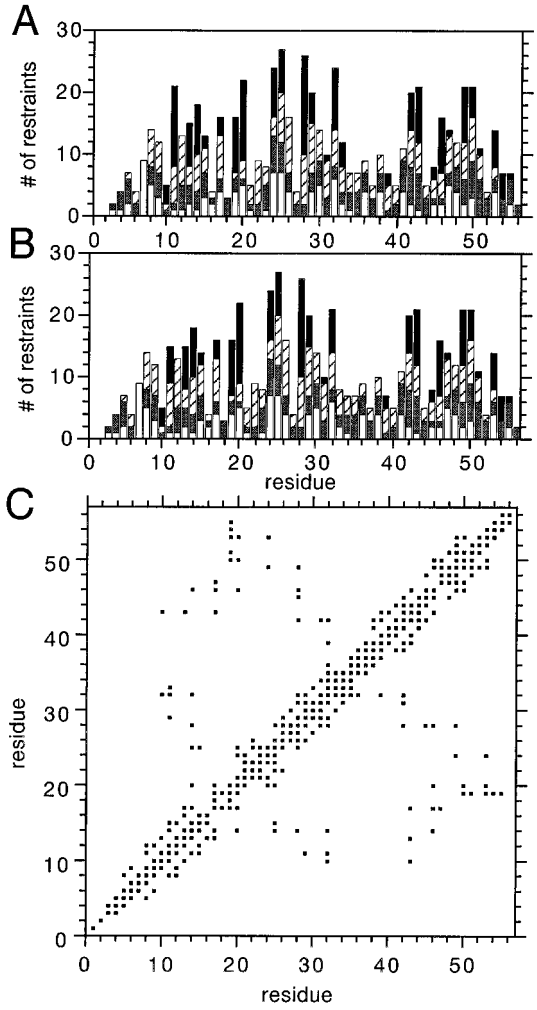

FIGURE 5: Number of NOE restraints per residue used in determining the structure of the E-domain: (A) E_{-60}; (B) E_{180}. Open bars indicate intraresidue NOEs; shaded bars indicate sequential NOEs; hatched bars indicate medium-range NOEs (between residues 2, 3, or 4 away in the sequence); and filled bars indicate long-range NOEs (between residues separated by >4 residues in the sequence). (C) NOE contact plot. A filled square indicates the presence of at least one NOE between protons from the connected residues. E_{-60} and E_{180} NOEs are shown above and below the diagonal, respectively.

connectivities (Figure 3); α-helical hydrogen bond restraints were added for those residues having slowed amide proton exchange rates and found from the initial structures to be in regions of regular α-helical structure. The restraints used to calculate the final structures include 383 NOE restraints that were nonredundant with covalent geometry (79 sequential, 101 medium range, and 82 long range), 34 ϕ and 19 χ_1 dihedral restraints, and 54 restraints for 27 hydrogen bonds, totaling 9.7 restraints per residue for residues 8−53. Fifty E-domain structures were calculated using the hybrid distance geometry/simulated annealing algorithm, DGII. All of these calculations converged to structures with low violations. The DG structures were further refined using rMD with DISCOVER as described in Materials and Methods.

When all NOEs were included in the calculation, the resulting structures exhibited good geometry throughout, except for the side chain of Phe11; the χ_1 angle for this residue was well-defined but in an unfavorable conformation of $-92 \pm 12°$. In the complexed state, Phe11 occupies the

Table 2: E-Domain Structural Statistics

	E_{-60}	$E_{-60mean}$[a]	E_{180}	$E_{180mean}$
rms deviation from exptl distance restraints (Å)				
NOE	0.006 ± 0.002 (381)	0.004 (381)	0.006 ± 0.001 (375)	0.004 (375)
H-bond	0.001 ± 0.001 (54)	0.000 (72)	0.000 ± 0.001 (54)	0.000 (72)
rms deviation from exptl dihedral restraints (deg)				
ϕ (34), χ_1 (19)	0.22 ± 0.05	0.14	0.21 ± 0.05	0.18
NOE distance violations				
0.1 Å > no. > 0.01 Å	8.7 ± 2.9	9	10.1 ± 2.6	9
no. > 0.1 Å	0.2 ± 0.4	0	0.2 ± 0.4	0
maximum (Å)	0.08 ± 0.03	0.04	0.07 ± 0.02	0.04
dihedral angle violations				
1° > no. > 0.1°	2.5 ± 1.1	3	2.4 ± 1.4	2
no. > 1°	1.0 ± 0.7	0	1.1 ± 0.9	1
maximum (deg)	1.2 ± 0.3	0.9	1.2 ± 0.2	1.2
rms deviations from idealized covalent geometry[b]				
bonds (Å) (852)	0.0051 ± 0.0001	0.0051	0.0051 ± 0.0001	0.0050
angles (deg) (1533)	1.40 ± 0.03	1.42	1.41 ± 0.04	1.34
planes (deg) (170)	1.64 ± 0.13	2.17	1.60 ± 0.11	1.89
energies (kcal·mol^{-1})				
$E_{restraint}$[c]	0.49 ± 0.24	0.21	0.46 ± 0.16	0.16
E_{bond}	7.0 ± 0.2	7.1	6.9 ± 0.3	6.7
E_{angle}	41.6 ± 2.0	42.2	41.7 ± 2.3	37.9
$E_{torsion}$	56.1 ± 2.5	61.0	55.2 ± 2.2	55.5
E_{plane}	0.90 ± 0.11	1.03	0.86 ± 0.09	0.83
E_{vdW}[d]	−211.8 ± 4.4	−218.2	−209.1 ± 6.3	−215.5
E_{elec}[e]	−182.7 ± 2.5	−190.3	−182.0 ± 2.3	−183.8
E_{total}	−316.5 ± 7.2	−326.9	−314.1 ± 8.9	−328.7

[a] The minimized mean is the structure obtained by restrained minimization of the mean coordinates, with the addition of 18 hydrogen bond restraints for 9 hydrogen bonds that are present in the majority of the final structures that had been calculated without them as input restraints, and involving amide protons with decreased solvent exchange rates. [b] Idealized covalent geometry is defined by the AMBER force field as implemented within DISCOVER. [c] The final values of the square-well NOE and dihedral angle potentials are calculated with force constants of 25 kcal·mol^{-1}·Å^{-2} and 100 kcal·mol^{-1}·rad^{-2}, respectively. [d] E_{vdW} is the Lennard-Jones van der Waals energy calculated with the all-atom AMBER force field and a 10 Å cutoff. [e] E_{elec} is calculated using a distance-dependent dielectric constant, $\epsilon = 4r$.

180° χ_1 rotamer and is buried in the interface (Deisenhofer, 1981); thus the conformation of Phe11 in the uncomplexed state warranted further investigation. The $^3J_{H^\alpha-H^\beta}$ coupling constants for Phe11, 6.5 and 9.2 Hz, are inconsistent with a χ_1 angle fixed at −92°. Assuming that the coupling constants are a weighted average resulting from the three low-energy χ_1 rotamers (−60°, 180°, +60°) gives two possible distributions of χ_1 with ratios −60°:180°:+60° of approximately 2:1:0 or 1:2:0 (Kessler et al., 1987). Measurement of the $^3J_{N-H^\beta}$ coupling constants from a homonuclear TOCSY spectrum acquired without ^{15}N decoupling (Montelione et al., 1989, 1992) gave −3.5 ± 0.5 Hz for the $^1H^\beta$ having the 6.5 Hz $^3J_{H^\alpha-H^\beta}$ coupling constant and −1 ± 1 Hz for the $^1H^\beta$ having the 9.2 Hz $^3J_{H^\alpha-H^\beta}$ coupling constant. Together, these data are consistent with Phe11 occupying χ_1 rotamers of −60° and 180° in a 2:1 ratio.

To account for both χ_1 conformations of Phe11 in the structure determination, we first calculated two sets of structures in which Phe11 χ_1 was fixed to either −60° or 180°, and the force constants on all NOE restraints involving Phe11 were reduced to 1 kcal·mol^{-1}·Å^{-2} to evaluate which NOEs were incompatible with each geometry. Two medium-range NOEs were consistently violated in the χ_1 −60° conformer, and eight medium- and long-range NOEs were consistently violated in the χ1 180° conformer. Specifically, the ring protons from Phe11 exhibit NOEs with the *pro-R* methyl protons of both Leu15 and Leu32 that are incompatible with a single structure. These NOEs are resolved and unambiguously assigned as shown in Figure 4.

Two new sets of structure calculations were then performed: one that excluded the NOEs conflicting with Phe11 $\chi_1 = -60°$ and the other excluding those conflicting with $\chi1 = 180°$ (Figure 5, Table S2). No χ_1 dihedral restraint was enforced for Phe11, and all NOE restraints were imposed with force constants of 25 kcal·mol^{-1}·Å^{-2}. In both calculations, Phe11 adopted a well-defined conformation, but they differed significantly in the resulting χ_1 value. In the first set (hereafter referred to as E_{-60}), Phe11 has $\chi_1 = -61.7 \pm 8.3°$; in the second set (E_{180}) Phe11 has $\chi_1 = -177.6 \pm 8.2°$. The 20 structures with the lowest restraint violation energies for each calculation of 50 structures were chosen to represent the solution structure of the E-domain.

Precision and Quality of the Structure Ensembles. Table 2 summarizes the structural statistics for the two E-domain ensembles. The structures satisfy the experimental restraints very well, as evidenced by the low restraint violation energies (E_{-60}, 0.49 ± 0.24 kcal·mol^{-1}; E_{180}, 0.46 ± 0.16 kcal·mol^{-1}); neither ensemble has any distance or dihedral angle violations greater than 0.12 Å or 1.6°, respectively. The atomic rms differences for backbone and heavy atoms and angular order parameters (Hyberts et al., 1992) were plotted to assess the precision of each ensemble of E-domain structures (Figure 6). Best-fit superpositions of residues 8−53 of the final two sets of structures on their respective mean coordinates are shown in Figure 7. The greatest disorder is present in the N- and C-termini, while the core of the molecule is well-defined with backbone atomic rms differences from the mean coordinates for residues 8−53 of 0.41 ± 0.06 Å (E_{-60}) and 0.35 ± 0.06 Å (E_{180}) (Table 3). The stereochemical quality of each ensemble was examined using the program PROCHECK (Laskowski et al., 1993). In the well-defined core of the molecule (residues 8−53), 90.0% (E_{-60}) and 90.4% (E_{180}) are located in the favorable region and 10.0% (E_{-60}) and 9.5% (E_{180}) in the acceptable region of ϕ, ψ space;

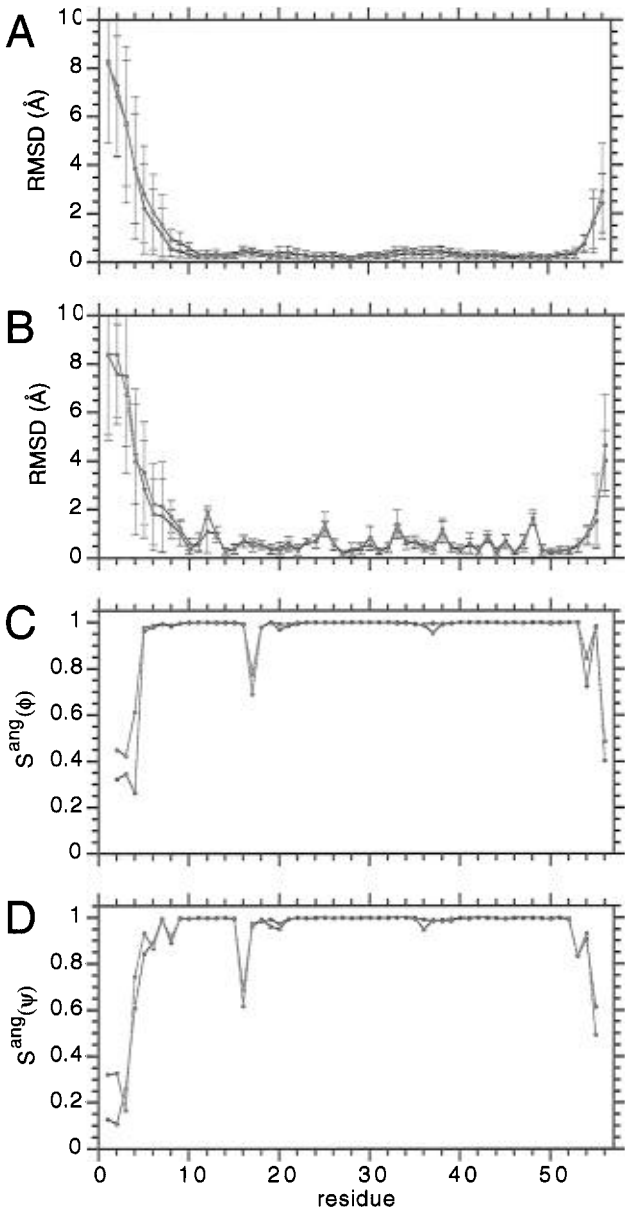

FIGURE 6: Atomic rms deviations (mean ± SD) of each set of 20 E-domain structures about the mean coordinates on a per residue basis for backbone atoms (N, C^{α}, C) (A) and all heavy atoms (B). Angular order parameters for ϕ (C) and ψ (D) dihedral angles calculated from each set of 20 structures. The E_{-60} ensemble is shown in blue and the E_{180} in red.

there are no residues in any of the 40 structures in the disallowed region and only one structure with one residue (Met17) in the generously allowed region.

DISCUSSION

Comparison of E_{-60} and E_{180} Ensembles. Despite the differing Phe11 side-chain orientations, E_{-60} and E_{180} represent very similar structures (Figure 7). The backbone atomic rms differences between structures in a given ensemble and the mean coordinates of the other ensemble are only slightly greater than those to its own mean coordinates (Table 3). Examination of interhelical angles also reveals no significant difference between E_{-60} and E_{180} ensembles; the mean values are slightly different, but the ranges of values observed within the ensembles overlap (Table 4). Thus, no significant conformational change need accompany repositioning of the phenyl ring of Phe11. In the following discussions, details of the structure apply equally well to E_{-60} and E_{180} unless stated otherwise.

Description of the Structure. The E-domain of protein A forms a compact three-helix bundle (Figure 7); helices 1, 2, and 3 comprise residues 8−15, 22−34, and 39−52, respectively [based on a Kabsch and Sander (1983) type analysis using the program PROCHECK (Laskowski et al., 1993)]. The helices are very well defined with backbone atomic rms differences from the mean coordinates of ≤0.19 Å when considered individually. A glycine residue is present in the middle of both helix 2 (Gly27) and helix 3 (Gly44), but no disruption from regular α-helical geometry is present in these helices. The three α-helices are interrupted by two type I turns involving residues 17−20 and 35−38 that are also well-defined locally with backbone atomic rms differences from the mean coordinates of ≤0.22 Å. All three proline residues are in the *trans* conformation, as evidenced by strong sequential $H^{\alpha}-H^{\delta}$ NOEs. Residues 5, 6, and 7 are included as part of helix 1 in 13/20, 14/20, and 20/20 E_{-60} structures and 7/20, 15/20, and 18/20 E_{180} structures, respectively, but they are not as well-defined as the core of the molecule. Residues 1−4 and 54−56 are disordered in the structures (Figures 6 and 7).

The side-chain $H^{\epsilon 21}$ protons of Gln24 and Gln53 resonate far downfield from the chemical shift typical of unstructured glutamines, at 8.14 and 8.56 ppm, respectively (Figure 2B, Table S1). These distinctive chemical shifts are conserved in the NMR spectra of both B- and Z-domains (Gouda et al., 1992; Lyons et al., 1993). Furthermore, these usually labile protons are protected from exchange with the solvent. In each ensemble of 20 structures, 12 have a hydrogen bond between Gln24 $H^{\epsilon 22}$ and Gln53 $O^{\epsilon 1}$, and 10 have a hydrogen bond between Gln53 $H^{\epsilon 22}$ and Gln24 $O^{\epsilon 1}$, although no hydrogen bonds involving side chains were included as restraints. The observed hydrogen bonds are consistent with the reduced proton/deuterium exchange rates and the unusual downfield chemical shifts observed for these side-chain amide protons. The structures suggest an additional role for the side-chain oxygen of Gln24, which is found hydrogen bonded to the backbone amide proton of Asn21 in 9 (E_{-60}) and 8 (E_{180}) of the final 20 structures. In addition, the side-chain oxygen of Asn21 is hydrogen bonded to the backbone amide proton of Gln24 in 17 (E_{-60}) and 13 (E_{180}) structures, indicating the presence of a classic N-terminal capping box (Harper & Rose, 1993). The hydrogen-bonding interactions involving Asn21, Gln24, and Gln53 that are observed in the E-domain structure are shown in Figure 8. Mutagenesis of Asn21, Gln24, and Gln53 confirms that both the N-cap and the Gln24/Gln53 interaction contribute to domain stability (E. Zhukovsky and L. G. Presta, unpublished results).

Additional amide protons protected from hydrogen/deuterium exchange that can be explained by their participation in hydrogen bonds in the E-domain structure ensemble include Phe11 H^{N}, Asn16 $H^{\delta 22}$, Met17 H^{N}, Asn19 H^{N} and $H^{\delta 22}$, Leu20 H^{N}, Gln38 H^{N}, and Gln53 H^{N}. Hydrogen bonds involving these protons were not included as restraints. The backbone amide protons of Phe11, Met17, and Gln53 are found in α-helical *(i, i* − 4) hydrogen bonds in 17, 9, and 18 E_{-60} structures, and 17, 6, and 18 E_{180} structures, respectively. The backbone amide protons of Leu20 and Gln38 form tight turn *(i, i* − 3) hydrogen bonds in 11 and 18 E_{-60} structures and 8 and 18 E_{180} structures, respectively. The side-chain $H^{\delta 22}$ of Asn16 caps the C-terminus of helix

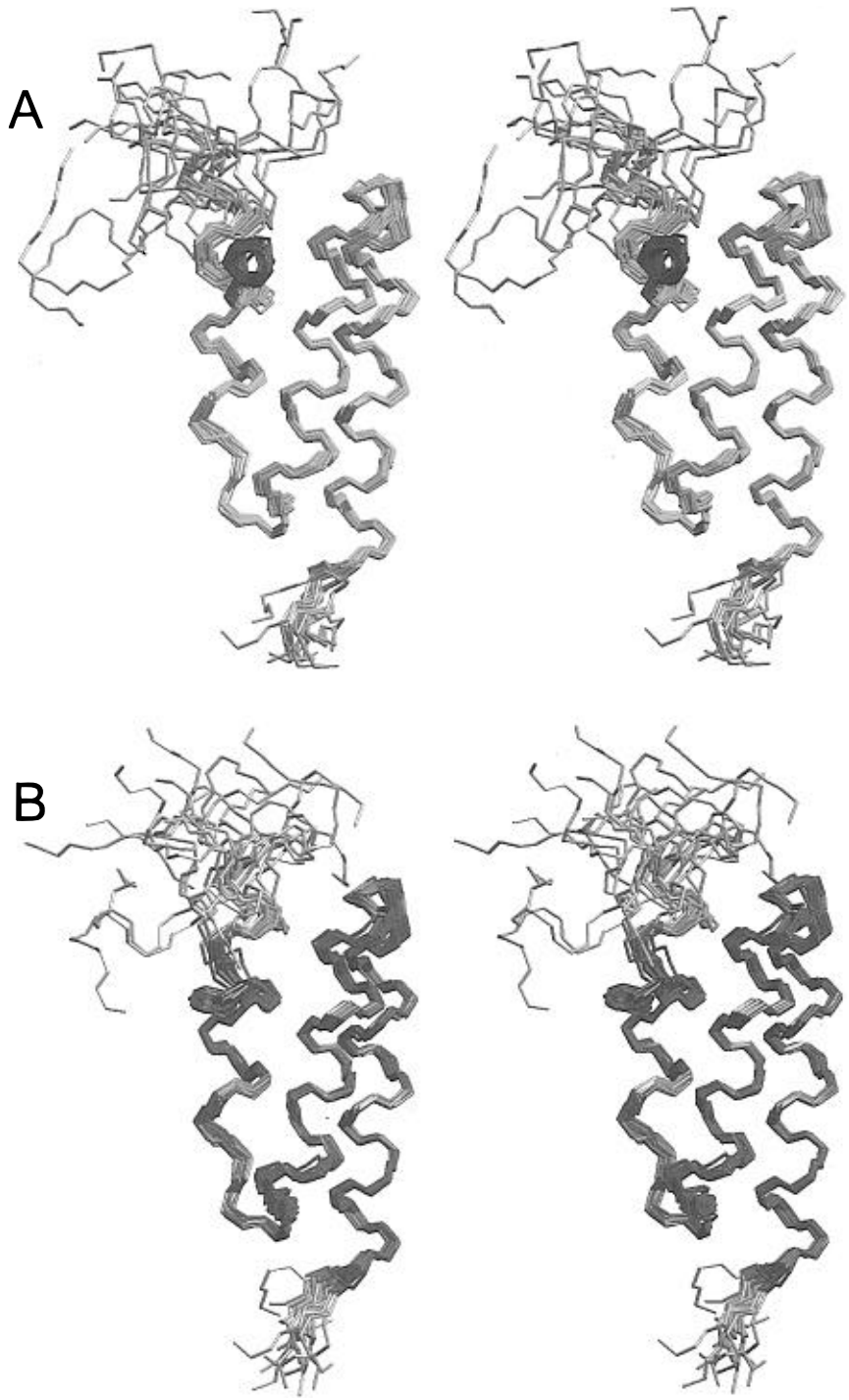

FIGURE 7: Stereoviews of the NMR structure of the E-domain. The final 20 E_{-60} structures are shown superposed using backbone atoms for residues 8−53. (A) E_{-60}; (B) E_{180}. Residues 1−7 and 54−56 are shown in gray, and the side chain for Phe11 is shown in red. This figure and Figures 8−10 were produced using INSIGHT II (Biosym Technologies, Inc.).

1 in 10 E_{-60} and 9 E_{180} structures by hydrogen bonding to the carbonyl oxygen of Tyr12. Asn19 $H^{\delta 22}$ hydrogen bonds to the carbonyl oxygen of Asn50 in 17 E_{-60} and 19 E_{180} structures, and Asn50 $O^{\delta 1}$ hydrogen bonds to the backbone amide proton of Asn19 in 19 E_{-60} and 20 E_{180} structures. The data are insufficient to uniquely define hydrogen-bonding partners for the remaining protected side-chain and backbone amide protons.

Comparison with the NMR Structure of the B-Domain. The E- and B-domains from protein A share 71% amino acid identity, differing in only 10 residues within the helical-bundle core (Figure 1). Thus, they are expected to have very similar three-dimensional structures. The E- and B-domain NMR structures were determined using similar numbers of restraints, yielding ensembles of structures with similar precision within the 3-helix bundle [0.52 ± 0.10 Å backbone (N, C^{α}, C, O) atomic rms difference from the mean coordinates for residues 7−52 of the B-domain; Gouda et al., 1992]. The secondary structure of the E-domain described herein is nearly identical to that observed in the NMR structure of the B-domain. However, there are significant differences in the tertiary structure; superposition of the backbone heavy atoms for residues 8−53 of the E-domain ensembles on the minimized mean structure of

Table 3: Atomic rms Differences (Å) with Respect to the Mean Coordinates[a] for Each Set of 20 E-Domain Structures

	E_{-60}		E_{180}	
aligned residues	backbone[b]	heavy atoms	backbone	heavy atoms
3-helix bundle (8−53)	0.41 ± 0.06	0.88 ± 0.09	0.35 ± 0.06	0.91 ± 0.06
mean vs min mean (8−53)	0.29	0.63	0.26	0.72
mean E_{-60} (8−53)[c]			0.46 ± 0.07	1.15 ± 0.08
mean E_{180} (8−53)[d]	0.51 ± 0.10	1.13 ± 0.07		

[a] The mean coordinates were calculated using a best fit superposition of residues 7−53. [b] Backbone atoms used were N, C^{α}, and C. [c] Atomic rms differences of the E_{180} structures with respect to the mean (not minimized) E_{-60} coordinates. [d] Atomic rms differences of the E_{-60} structures with respect to the mean E_{180} coordinates.

Table 4: Comparison of E-Domain Structures with B-Domain NMR and B-Domain/Fc Complex X-ray Structures

	Backbone Atomic rms Differences (Å) between E-Domain and B-Domain Structures				
aligned residues	E_{-60}/B_{NMR}[a]	E_{180}/B_{NMR}	$E_{-60}/B_{X\text{-}ray}$[b]	$E_{180}/B_{X\text{-}ray}$	$B_{NMR}/B_{X\text{-}ray}$
helix 1 (8−15)	0.56 ± 0.06	0.51 ± 0.04	0.39 ± 0.07	0.35 ± 0.06	0.56
helix 2 (22−34)	0.97 ± 0.03	0.91 ± 0.04	0.41 ± 0.02	0.42 ± 0.02	1.01
helix 3 (39−52)	0.63 ± 0.04	0.60 ± 0.05	NA[c]	NA	NA
helix 1/helix 2	1.58 ± 0.12	1.45 ± 0.05	0.75 ± 0.08	0.60 ± 0.08	1.43
helix 1/helix 3	1.24 ± 0.15	1.09 ± 0.06	NA	NA	NA
helix 2/helix 3	1.19 ± 0.04	1.22 ± 0.06	NA	NA	NA
residues 8−34	1.65 ± 0.12	1.53 ± 0.06	0.85 ± 0.09	0.74 ± 0.07	1.51
3-helix (8−53)	1.52 ± 0.11	1.44 ± 0.06	NA	NA	NA

	Interhelical Angles (deg)[d]		
structure	helix 1/helix 2	helix 1/helix 3	helix 2/helix 3
E_{-60}	168 ± 8 (156 to −174)	16 ± 3 (9 to 22)	174 ± 3 (167 to 179)
E_{180}	178 ± 4 (168 to −173)	19 ± 4 (10 to 25)	172 ± 3 (166 to 178)
B_{NMR}	−150	38	177
$B_{X\text{-}ray}$	179	NA	NA

[a] B_{NMR} refers to the minimized mean coordinates from the NMR structure of the B-domain (Gouda et al., 1992). [b] $B_{X\text{-}ray}$ refers to the structure of the B-domain in complex with Fc (Deisenhofer, 1981; PDB accession code 1FC2). [c] Not applicable. [d] Interhelical angles were measured using the method of Chothia et al. (1981). Residues 8−15, 22−34, and 39−52 were used for helices 1, 2, and 3, respectively, for all NMR structures measured; residues 7−15 and 22−34 were used for helices 1 and 2, respectively, of $B_{X\text{-}ray}$. The mean and standard deviation for the angles are indicated; the range of angles observed within the ensemble is given in parentheses.

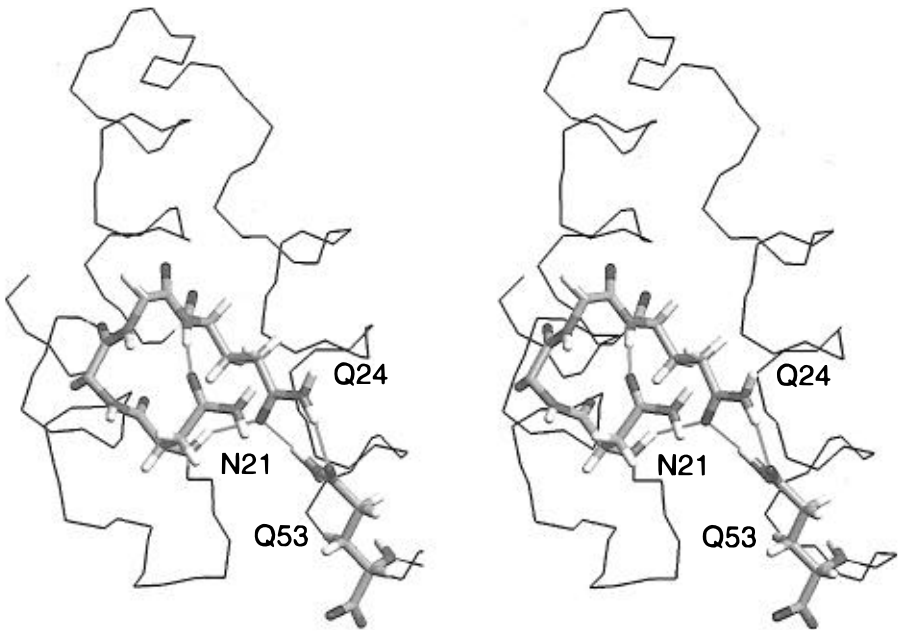

FIGURE 8: Hydrogen-bonding interactions involving the side chains of Asn21, Gln24, and Gln53. A stereoview of the E_{180} minimized mean structure is shown. Hydrogen bonds are indicated by orange lines.

the B-domain yields rms displacements of 1.52 ± 0.11 and 1.44 ± 0.06 Å for E_{-60} and E_{180}, respectively (Table 4, Figure 9A). The major differences between the B- and E-domain structures are the relative orientations of helix 1 with respect to helices 2 and 3; the mean helix 1/helix 2 angle differs by ~30°, and the mean helix 1/helix 3 angle differs by ~20° (Table 4). The significance of these differences is not apparent, although we note that the agreement between the structures and the experimentally derived restraints used to calculate them is significantly greater for the E-domain than

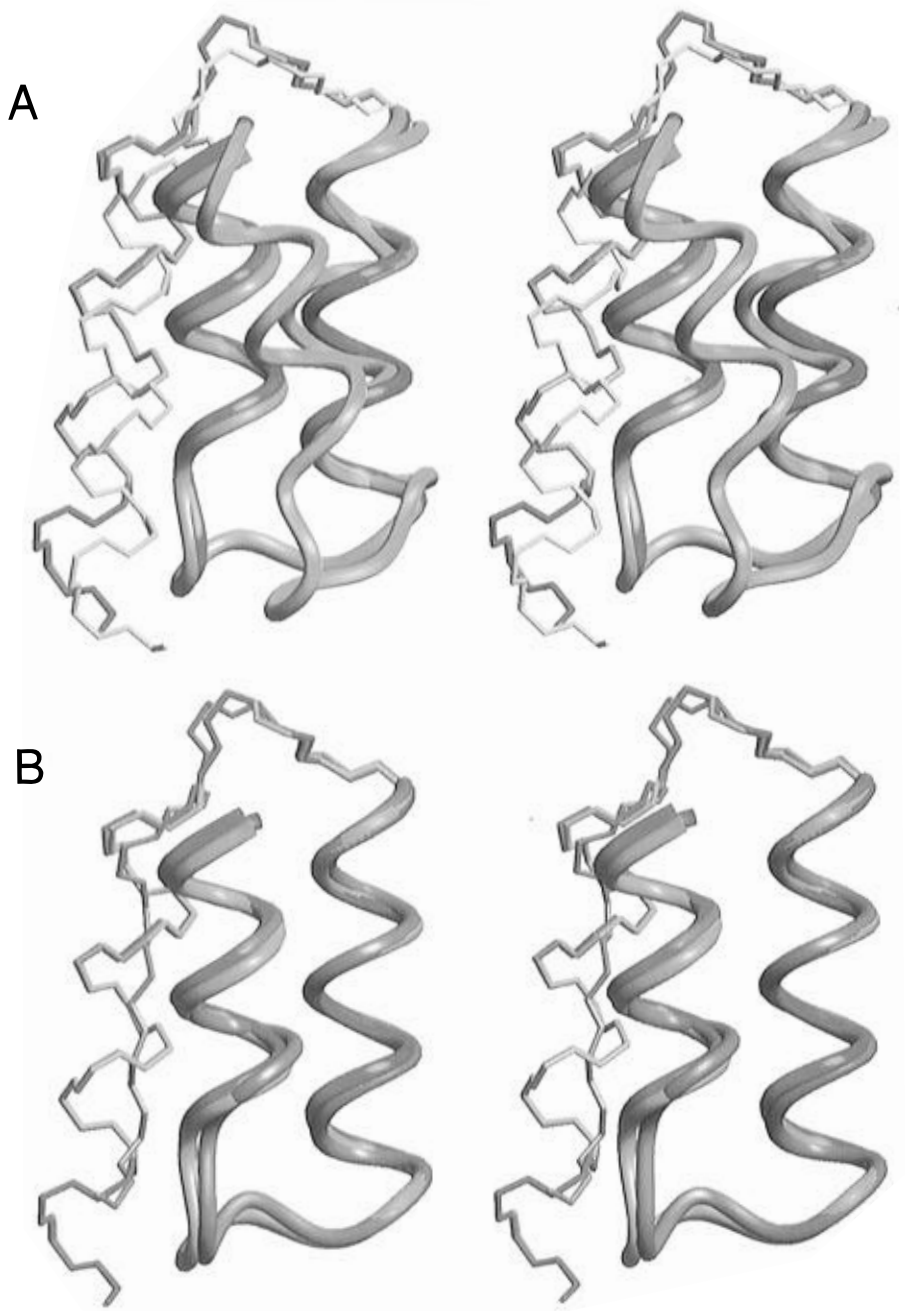

FIGURE 9: Minimized mean coordinates of the NMR structure of the E-domain, E_{-60} (cyan) and E_{180} (dark blue), superposed on (A) the minimized mean coordinates of the NMR structure of the B-domain (yellow; Gouda et al., 1992) and (B) the X-ray structure of the B-domain in complex with Fc (pink, PDB accession code 1FC2; Deisenhofer, 1981). The view shown in this figure has all structures superposed on helix 2 only (residues 22−34) to emphasize the relative orientation of helix 1 with respect to helix 2. Residues 8−34 are shown as tubes; residues 1−7 and 54−56 are not shown.

for the B-domain [rms deviations from experimental distance and dihedral restraints of 0.006 ± 0.002 Å and 0.22 ± 0.05°, respectively, for the E-domain (Table 2) compared with 0.055 ± 0.003 Å and 1.2 ± 0.5°, respectively, for the B-domain (Gouda et al., 1992)]. In this regard, the recent preliminary structure of the B-domain variant, Z-domain, also differs significantly from the free B-domain structure with respect to the helix 1/helix 2 angle (Jendeberg et al., 1996). The interhelical angles of the Z-domain are more similar to the present E-domain structures. However, a more detailed comparison would be premature and awaits refined coordinates for the Z-domain structure.

To test the dependence of the observed E-domain helical angles on the particular experimental restraints employed, further structure calculations were performed in which restraints were randomly removed. All E_{-60} restraints (NOE distance, hydrogen bond distance and dihedral angle) were randomly partitioned into 10 groups of equal size, and 10 ensembles were calculated with restraints from which one of these groups was omitted. This is similar to a jackknife statistical test except that the restraints are tested in groups rather than individually (Brünger et al., 1993). All calculations converged to structures with low violations and had backbone atomic rms differences from the E_{-60} mean coordinates (calculated using all restraints) of ~0.5 Å for residues 8−53. The resulting average helix 1/helix 2 angle for each test ensemble ranged from 162 to 169°, indicating that no single restraint is responsible for the resulting interhelical angles reported here for the E-domain and that the ensemble is an *accurate* representation of the structure.

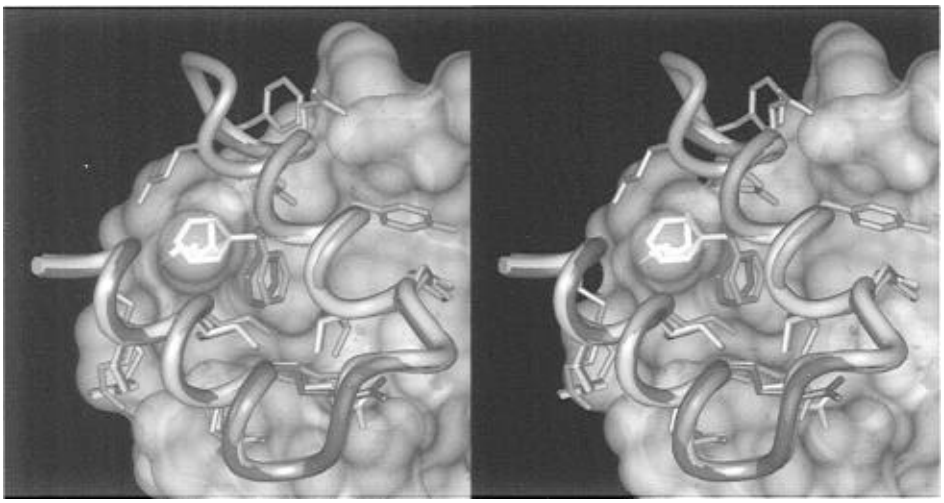

FIGURE 10: Comparison of the Fc-binding region of the B-domain (pink) in complex with Fc (shown as a transparent Connolly surface) with the same region of the E-domain, E_{-60} (cyan) and E_{180} (dark blue). The minimized mean coordinates of the E-domain are shown superposed on the B-domain using residues 7−34. The backbones of residues 3−34 for the B-domain and residues 7−34 for the E-domain are represented as tubes; the view shown has helix-1 in the upper right and helix 2 in the lower left of the figure. B-Domain side chains are shown for residues that contact Fc in the structure of the complex (Phe3, Gln7, Gln8, Asn9, Phe11, Tyr12, Leu15, His16, Arg25, Asn26, Ile29, Gln30, Lys33). The corresponding side chains of the E-domain that are also well-defined in the NMR structure [$S^{ang}(\chi_1) > 0.9$; Phe11, Leu15, Asn16, Arg25, Asn26, Ile29, Gln30] are shown. Also shown within the transparent surface is Fc residue Ile253 (white). Note that the phenyl ring of Phe11 in E_{-60} occupies the same space as Ile253, whereas Phe11 in E_{180} overlaps Phe11 in the structure of the complex which fills a pocket on the Fc surface.

Comparison with the Crystal Structure of the B-Domain/Fc Complex. As mentioned in the introduction, the crystal structure of the B-domain in complex with Fc lacks the third α-helix. This is clearly the major difference between the E-domain structure and the crystal structure. However, since mounting evidence supports the notion that the third helix remains intact in the Fc-bound state (Gouda et al., 1992; Jendeberg et al., 1996), we focus only on a comparison of the regions containing residues 8−34, which are well-defined in both the E-domain and the B-domain/Fc complex structures and include nearly all residues that contact Fc. Comparing residues 8−34 of the Fc-bound B-domain and each E-domain structure ensemble gives backbone atomic rms differences of 0.85 ± 0.09 Å (E_{-60}) and 0.74 ± 0.07 Å (E_{180}) (Table 4, Figures 9B and 10). This is likely within the accuracy limits of the structures (Zhao & Jardetzky, 1994). The angle between helices 1 and 2 is also not significantly different (Table 4). However, comparing the locations of ordered side chains in the E-domain ensembles [$S^{ang}(\chi_1) > 0.9$] with the corresponding side chains in the Fc-bound B-domain reveals a significant difference for Phe11 in the E_{-60} ensemble.

In the uncomplexed E-domain, the phenyl ring of Phe11 exists clearly in two conformations; in E_{-60}, it packs against the three-helix bundle ($\chi_1 = -61.7 \pm 8.3°$), and in E_{180}, it points away from the bundle ($\chi_1 = -177.6 \pm 8.2°$). In the Fc-bound B-domain the side chain points away from the bundle ($\chi_1 = 161°$), interacts with Fc, and leaves a cavity in the bundle that is filled by Ile253 from the CH_2 domain of Fc (Figure 10). The E_{180} ensemble is indistinguishable from the bound state, but the E_{-60} conformer would require reorientation of Phe11 prior to binding in order to avoid a steric clash between this side chain and the side chain of Ile253 (Figure 10). We propose, therefore, that the conformational change suggested by slowed on-rates for E, B, and Z domains (Table 1; Jendeberg et al., 1995) results from a repositioning of the side chain of Phe11. A large change in the helix 1/helix 2 angle does not appear to occur upon complex formation, although a small change (<10°, within the precision of the structures) could accompany the phenylalanine reorientation.

In summary, we have determined the three-dimensional structure of the uncomplexed E-domain from protein A by NMR spectroscopy. The structure forms a compact three-helix bundle similar to that found for the B-domain and Z-domain (Gouda et al., 1992; Jendeberg et al., 1996). Under conditions used for structure determination (25 °C, pH 5.7), Phe11 was found to populate two conformations, with χ_1 values of −60° and 180° in a 2:1 ratio. Comparison with the Fc-bound B-domain crystal structure reveals no significant difference in the relative orientation of helices 1 and 2 but does show a difference in the side-chain orientation of Phe11 with that of the E_{-60} ensemble. The phenyl ring of Phe11 in E_{-60} occupies the same space as that of Ile253 from Fc in the structure of the complex (Figure 10); thus only when Phe11 χ_1 is 180° will the complex as seen in the B-domain/Fc crystal structure be formed. The structure of the uncomplexed E-domain presented here not only provides a more detailed look at the conformational change involved in binding Fc fragments but will serve as a starting point to examine the molecular nature of Fv complex formation. The E-domain/Fv complex is amenable to study by NMR, and experiments to examine this complex are underway.

ACKNOWLEDGMENT

The authors thank Dr. Ichio Shimada for providing coordinates for the minimized mean B-domain NMR structure, Dr. Gaetano Montelione for providing unpublished Z-domain coordinates, Dr. Andrew Braisted for assisting with the BIAcore measurements, Joshua Theaker for providing the software to measure helix angles, Dr. Neil Jacobsen, in conjunction with Joshua Theaker, for implementing the curve fitting algorithm into FELIX for measuring coupling constants from antiphase cross-peaks in a COSY spectrum, Dr. Beth Gillece-Castro for obtaining the mass spectrometry

results, Dr. Leonard Presta for constructing the B-domain plasmid, and Dr. Bart de Vos for critical reading of the manuscript.

SUPPORTING INFORMATION AVAILABLE

A table containing all ^{1}H and ^{15}N resonance assignments and a table listing NOE restraints that were excluded specifically from E_{-60} or E_{180} structure calculations (4 pages). Ordering information is given on any current masthead page.

REFERENCES

Akke, M., Carr, P. A., & Palmer, A. G. (1994) *J. Magn. Reson. B 104*, 298−302.

Aue, W. P., Bartholdi, E., & Ernst, R. R. (1975) *J. Chem. Phys. 64*, 2229−2246.

Bax, A., & Davis, D. G. (1985) *J. Magn. Reson. 65*, 355−360.

Bodenhausen, G., Kogler, H., & Ernst, R. R. (1984) *J. Magn. Reson. 58*, 370−388.

Braisted, A. C., & Wells, J. A. (1996) *Proc. Natl. Acad. Sci. U.S.A. 93*, 5688−5692.

Braunschweiler, L., & Ernst, R. R. (1983) *J. Magn. Reson. 53*, 521−528.

Braunschweiler, L., Bodenhausen, G., & Ernst, R. R. (1983) *Mol. Phys. 48*, 535−560.

Brünger, A. T., Clore, G. M., Gronenborn, A. M., & Karplus, M. (1986) *Proc. Natl. Acad. Sci. U.S.A. 83*, 3801−3805.

Brünger, A. T., Clore, G. M., Gronenborn, A. M., Saffrich, R., & Nilges, M. (1993) *Science 261*, 328−331.

Capon, D. J., Chamow, S. M., Mordenti, J., Marsters, S. A., Gregory, T., Mitsuya, H., Byrn, R. A., Lucas, C., Wurm, F. M., Groopman, J. E., Broder, S., & Smith, D. H. (1989) *Nature 337*, 525−531.

Cavanagh, J., & Rance, M. (1992) *J. Magn. Reson. 96*, 670−678.

Cavanagh, J., Palmer, A. G., Wright, P. E., & Rance, M. (1991) *J. Magn. Reson. 91*, 429−436.

Chang, C. N., Rey, M., Bochner, B., Heyneker, H., & Gray, G. (1987) *Gene 55*, 189−196.

Chazin, W. J., & Wright, P. E. (1988) *J. Mol. Biol. 202*, 623−636.

Chazin, W. J., Rance, M., & Wright, P. E. (1988) *J. Mol. Biol. 202*, 603−622.

Chothia, C., Levitt, M., & Richardson, D. (1981) *J. Mol. Biol. 145*, 215−250.

Clore, G. M., Brünger, A. T., Karplus, M., & Gronenborn, A. M. (1986) *J. Mol. Biol. 191*, 523−551.

Davis, D. G. (1989) *J. Magn. Reson. 81*, 603−607.

Deisenhofer, J. (1981) *Biochemistry 20*, 2361−2370.

Deisenhofer, J., Jones, T. A., Huber, R., Sjödahl, J., & Sjöquist, J. (1978) *Hoppe-Seyler's Z. Physiol. Chem. 359*, 975−985.

Gouda, H., Torigoe, H., Saito, A., Sato, M., Arata, Y., & Shimada, I. (1992) *Biochemistry 31*, 9665−9672.

Harper, E. T., & Rose, G. D. (1993) *Biochemistry 32*, 7605−7609.

Havel, T. F. (1991) *Prog. Biophys. Mol. Biol. 56*, 43−78.

Hyberts, S. G., Goldberg, M. S., Havel, T. F., & Wagner, G. (1992) *Protein Sci. 1*, 736−751.

Jendeberg, L., Persson, B., Andersson, R., Karlsson, R., Uhlén, M., & Nilsson, B. (1995) *J. Mol. Recognit. 8*, 270−278.

Jendeberg, L., Tashiro, M., Tejero, R., Lyons, B. A., Uhlén, M., Montelione, G. T., & Nilsson, B. (1996) *Biochemistry 35*, 22−31.

Johnsson, B., Löfås, S., & Lindquist, G. (1991) *Anal. Biochem. 198*, 268−277.

Kabsch, W., & Sander, C. (1983) *Biopolymers 22*, 2577−2637.

Karlsson, R., Michaelson, A., & Mattson, A. (1991) *J. Immunol. Methods 145*, 229−240.

Kessler, H., Griesinger, C., & Wagner, K. (1987) *J. Am. Chem. Soc. 109*, 6927−6933.

Kessler, H., Griesinger, C., Lautz, J., Müller, A., van Gunsteren, W. F., & Berendsen, H. J. C. (1988) *J. Am. Chem. Soc. 110*, 3393−3396.

Koning, T. M. G., Boelens, R., & Kaptein, R. (1990) *J. Magn. Reson. 90*, 111−123.

Kumar, A., Ernst, R. R., & Wüthrich, K. (1980) *Biochem. Biophys. Res. Commun. 95*, 1−6.

Langone, J. J. (1982) *Adv. Immunol. 32*, 157−252.

Laskowski, R. A., MacArthur, M. W., Moss, D. S., & Thornton, J. M. (1993) *J. Appl. Crystallogr. 26*, 283−291.

Lyons, B. A., Tashiro, M., Cedergren, L., Nilsson, B., & Montelione, G. T. (1993) *Biochemistry 32*, 7839−7845.

Marion, D., & Wüthrich, K. (1983) *Biochem. Biophys. Res. Commun. 113*, 967−974.

Marion, D., Ikura, M., Tschudin, R., & Bax, A. (1989) *J. Magn. Reson. 85*, 393−399.

Messerle, B. A., Wider, G., Otting, G., Weber, C., & Wüthrich, K. (1989) *J. Magn. Reson. 85*, 608−613.

Moks, T., Abrahmsen, L., Nilsson, B., Hellman, U., Sjöquist, J., & Uhlén, M. (1986) *Eur. J. Biochem. 156*, 637−643.

Montelione, G. T., Winkler, M. E., Rauenbuehler, P., & Wagner, G. (1989) *J. Magn. Reson. 82*, 198−204.

Montelione, G. T., Emerson, S. D., & Lyons, B. A. (1992) *Biopolymers 32*, 327−334.

Neri, D., Szyperski, T., Otting, G., Senn, H., & Wüthrich, K. (1989) *Biochemistry 28*, 7510−7516.

Nilsson, B., Moks, T., Jansson, B., Abrahmsén, L., Elmblad, A., Holmgren, E., Henrichson, C., Jones, T. A., & Uhlén, M. (1987) *Protein Eng. 1*, 107−113.

Press, W. H., Flannery, B. P., Teukolsky, S. A., & Vetterling, W. T. (1986) *Numerical Recipes. The Art of Scientific Computing*, Cambridge University Press, Cambridge.

Rance, M., & Byrd, R. A. (1983) *J. Magn. Reson. 54*, 221−240.

Rance, M., & Wright, P. E. (1986) *J. Magn. Reson. 66*, 372−378.

Reilly, D., & Fairbrother, W. J. (1994) *J. Biomol. NMR 4*, 459−462.

Senn, H., Werner, B., Messerle, B. A., Weber, C., Traber, R., & Wüthrich, K. (1989) *FEBS Lett. 249*, 113−118.

Tashiro, M., & Montelione, G. T. (1995) *Curr. Opin. Struct. Biol. 5*, 471−481.

Torigoe, H., Shimada, I., Saito, A., Sato, M., & Arata, Y. (1990) *Biochemistry 29*, 8787−8793.

Tropp, J. (1980) *J. Chem. Phys. 72*, 6035−6043.

Uhlén, M., Guss, B., Nilsson, B., Gatenbeck, S., Philipson, L., & Lindberg, M. (1984) *J. Biol. Chem. 259*, 1695−1702.

Wagner, G., Braun, W., Havel, T. F., Schaumann, T., Go, N., & Wüthrich, K. (1987) *J. Mol. Biol. 196*, 611−639.

Weiner, S. J., Kollman, P. A., Case, D. A., Singh, U. C., Ghio, C., Alagona, G., S. Profeta, J., & Weiner, P. (1984) *J. Am. Chem. Soc. 106*, 765−784.

Weiner, S. J., Kollman, P. A., Nguyen, D. T., & Case, D. A. (1986) *J. Comput. Chem. 7*, 230−252.

Wüthrich, K. (1986) *NMR of Proteins and Nucleic Acids*, J. Wiley and Sons, New York.

Wüthrich, K., Billeter, M., & Braun, W. (1983) *J. Mol. Biol. 169*, 949−961.

Zhao, D., & Jardetzky, O. (1994) *J. Mol. Biol. 239*, 601−607.

BI961409X